International Journal of Research in Advent Technology, Vol.7, No.5, May 2019
E-ISSN: 2321-9637
Available online at www.ijrat.org

Preparation and Microstructure Characterization of Ti-Base Different Metal Nitrides by Mechanical Alloying: A Brief Review

Ujjwal Kumar Bhaskar [1] and S.K. Pradhan[2]
[1]*Dept. of Physics, Sreegopal Banerjee College, Bagati, Magra, Hooghly-712148, India.*
[2]*Dept. of Physics, The University of Burdwan, Golapbag, Burdwan-713104*
Email: ukb1975@yahoo.com

Abstract- The nanocrystalline Ti-base metal nitrides having cubic structure $Ti_{0.9}M_{0.1}N$ (M= Al, C, B, Ni, Si) were synthesized at room temperature by mechanical alloying the ingredients powder materials under a nitrogen environment. The stoichiometric $Ti_{0.9}M_{0.1}N$ (cubic) phase initiated after 1h of milling and formed completely after 5h to 9h of milling depending upon the nature of doping materials. Microstructures of all ball-milled samples were characterized by analyzing the respective XRD patterns employing the Rietveld structure and microstructure refinement method. Microstructures of the prepared materials were also characterized by TEM micrograph to correlate the results obtained from the XRD pattern analysis. The effects of inclusion of different intermediate solute materials on the microstructure of the prepared materials were studied in this review article.

Keywords: Nanocrystalline; Rietveld; Microstructure; Phase transitions; Gas-solid reaction.

1. INTRODUCTION

Metal nitrides specially Ti-base metal nitrides are in the centre of attraction due to their high hardness and have potential industrial applications as coating materials. Of these, titanium nitride (TiN) has been studied quite widely because of its smart attributes, such as high hardness (2000 kg/mm^2), good electrical conductivity and high melting temperature (3000^{0}C) [1-3]. The metal nitrides find its applications such as coatings on cutting tools for obtaining improved hardness and wear resistance [4-8]. The mechanical properties of titanium carbide based cermets can be improved by adding extremely dispersed TiN [9]. TiN thin film is able to prevent aluminium diffusion into silicon in Al-TiN-Si trilayers at up to 550^{0}C [10].

$Ti_{0.57}Al_{0.43}N$ coating shows good thermal stability and can be used as a temperature controlling unit for the satellite [11]. TiAlN shows potential application as the upper electrode for dynamic random access memory (DRAM) devices [12]. TiAlN coating possesses high oxidation resistance at elevated temperatures up to 1075K [13]. The hardness of $Ti_{1-x}Al_xN$ coatings can reach a maximum value of 40 GPa when x is of 0.5–0.7 [14].

Ti(C,N) cermets possess high hardness, thermal stability, thermal conductivity, excellent creep resistance and wear resistance. Ti(C,N)-based cermets have been successfully utilized for high-performance wear parts and semi-finishing or finishing cutting tools [15]. The properties of TiCN-based cermets are intensively dependent on their chemical compositions and microstructure [16,17]. Gómez et. al. studied the influence of different parameters as the chemical composition and particle size of the metal matrix on TiCN-reinforced Fe-based composites [18]. Liu et. al. reveal the microstructure of interface and the relation between interface mixing and hardening mechanism in TiN/CNx multilayer films [19].

The nanostructured Ti-Si-N coating fabricated by PVD or CVD method have attracted greatly due to their high hardness of (up to 50 GPa) [20,21], thermal stability up to 800^{0}C [22] and excellent corrosion resistance [23]. With the introduction of Si into TiN, the hardness increased and the grain size decreased dramatically [20].

H. R. Stock et al studied the composition, morphology and hardness of Ti-Ni-N coatings deposited by unbalanced reactive magnetron sputtering [24].

In the present work, Ti-base different metal nitrides have been synthesized by mechanical alloying and studied the influences of intermediate doped material on the microstructure of the prepared sample.

2. EXPERIMENTAL

To synthesize the single-phase nanocrystalline $Ti_{0.9}M_{0.1}N$ (M= Al, C, Si, Ni) materials, the M (M= Al, C, Si, Ni) powder (purity 99.5%, Alfa Aesar) and α-Ti powder (purity 99.5%, Alfa Aesar) were taken at per molar ratio in a nitrogen-filled chrome-steel bowl and was ball-milled in a planetary ball-milling machine (Model P-5, Fritsch, Germany) for 1h to 9h time duration. The milling process was paused for 30min to restore the fresh nitrogen inside the bowl. X-ray powder diffraction patterns of the prepared nano-structured $Ti_{0.9}M_{0.1}N$ powder materials were recorded in step scan mode with step size 0.02^0 2θ and counting

time 2s/step from an X-ray powder diffractometer (consisting of a PW 3710 mpd controller, PW 1050/37 goniometer, and a proportional counter) operated at 20mA and 40KV using Ni-filtered CuKα radiation. TEM micrographs and SEAD patterns of the sample were obtained using an HRTEM (FEI, TECNAI G2 20, TWIN) operated at 200KV.

3. METHODOLOGY

A specially designed Rietveld software, MAUD [25] was employed to analyze the XRD patterns of unmilled and ball-milled samples. Structure and microstructure parameters like lattice parameters, mole fraction, r.m.s. lattice strain, particle size etc of the prepared materials were refined according to Rietveld analysis [25-32] to obtain the optimum values of these parameters by fitting the experimental XRD patterns of the respective samples through the successive refinement of the simulated XRD patterns. The theoretical XRD patterns were simulated by considering the presence of α-Ti (hcp, sp. gr. $P6_3/mmc$, a= 0.29508nm c= 0.46855 nm), M (Al, C, Si, Ni) and $Ti_{0.9}M_{0.1}N$ (fcc, sp. gr. Fm-3m, a= 0.4235 nm, the lattice constant of TiN) phases as precursors including parameters of diffraction optic effects, instrumental factors and other specimen characteristics.

4. RESULTS AND DISCUSSION

XRD patterns of 9h ball-milled TiN and $Ti_{0.9}M_{0.1}N$ (M= Al, C, Si, Ni) powder materials are shown in Fig. 1. The formation of TiN (cubic, ICDD PDF # 38-1420) phase was clearly noticed in the XRD pattern of 9h milled powder with the appearance of most intense (200) ($2\theta \sim 42.6^0$) and (111) reflections. TiN phase formed completely after 9h of milling whereas TiMN phase formed after 5h to 7h of milling time. The cubic Ti(C,N) (ICSD# 37402) phase (same cubic structure as TiN) was formed completely from the α-Ti-based interstitial solid solution. All reflections of Ti(CN) phase were sufficiently broaden which may be due to both small particle size and lattice strain developed inside the lattice due to constant fracture and re-welding mechanism of mechanical alloying (MA). A similar type of peak broadening was also observed in the TiAlN, TiSiN and TiNiN phases. It is to be noted that peak broadening of $Ti_{0.9}M_{0.1}N$ phases increases with the increase of atomic number of intermediate solutes which may be due to the substitution of Ti atoms (atomic radius =0.86Å) by smaller M (C, Al, Si, Ni) atoms.

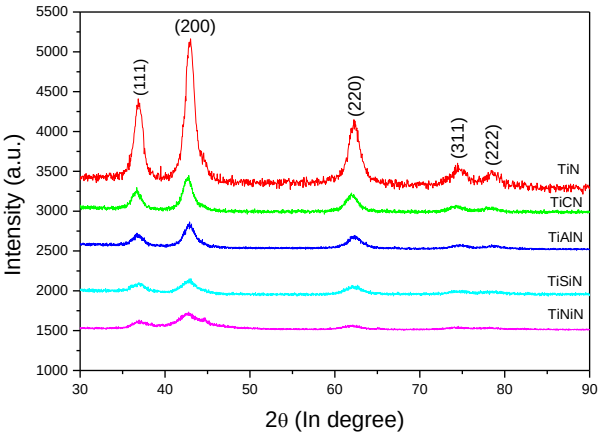

Fig. 1. X-ray powder diffraction patterns of ball-milled TiN and TiMN powders.

Variation of the lattice parameter of TiN and $Ti_{0.9}M_{0.1}N$ phases with increasing milling time is shown in Fig. 2. TiN phase initiated with a comparatively large value of lattice parameter and it decreased rapidly from 1h to 3h of milling which is due to continuous absorption of nitrogen inside the α-Ti lattice.

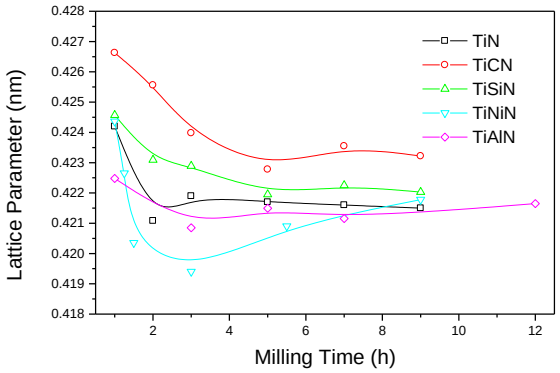

Fig.2. Variation of lattice parameters of TiN and TiMN phases with increasing milling time.

The lattice parameter of TiN phase remained unchanged after 3h of milling which indicated that the N-concentration in TiN phase became saturated after 3h of milling. The lattice of cubic (Ti, Al)N phase was formed after 1h of milling with significantly less value from that of cubic TiN phase. It implies that ~0.1 mol fraction of α-Ti atoms was occupied by the same amount of Al atoms with a smaller radius. After formation, lattice parameter of (Ti,Al)N phase contracted continuously in the course of milling, like the TiN phase. The similar kind variation of lattice parameter was also observed in case of Ti(CN), TiSiN and TiNiN phases. After 1h of milling, contraction in the lattice parameter of $Ti_{0.9}M_{0.1}N$ phases may be

explained for one or more of the following reasons: (a) cold-working caused due to high impulsive collision force on $Ti_{0.9}M_{0.1}N$ during milling, (b) constant re-arrangement of Ti and M atomic positions inside the lattice due to continuous diffusion of smaller N (ionic radius =0.13Å) atoms to achieve a stable atomic configuration and (c) annealing effect on imperfect $Ti_{0.9}M_{0.1}N$ lattice to shift it forward to a perfect lattice by thermal agitation of atoms during milling.

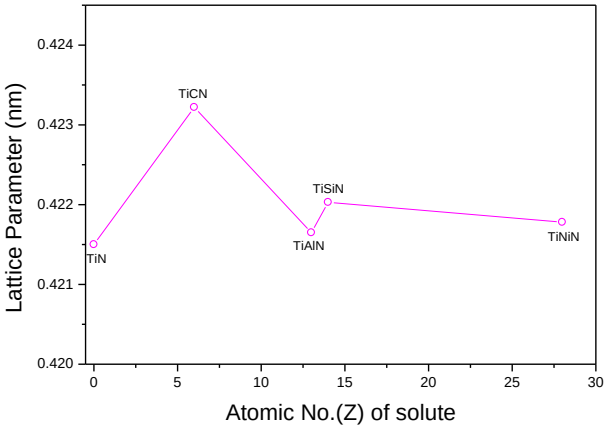

Fig.3. Variation of lattice parameter of TiMN phases with atomic number of solute.

Fig. 3 shows the variation of lattice parameter $Ti_{0.9}M_{0.1}N$ phases with an increasing atomic number of the solute. Lattice parameter of binary TiN and TiC [33] are 0.4215 nm and 0.43187 nm respectively but that of $Ti_{0.9}C_{0.1}N$ is 0.42322 nm. It is evident from the data of lattice parameter of Ti(C,N) phase that both C and N atoms were present in the lattice and concentration of C was less in comparison to N. In other words, some of the N atoms of TiN phase was replaced by the larger C atoms and $Ti_{0.9}C_{0.1}N$ phase was formed. Lattice parameter of TiAlN phase expanded slightly from that of TiN phase which was caused due to replacement of smaller N^{3+} ion (ionic radius = 0.16Å; CN=6) by the bigger Al^{3+} (ionic radius 0.53 Å; CN=6). Lattice expansion of TiNiN phase from that of TiN phase also caused due to the substitution of smaller N^{3+} ion by the bigger Si^{4+} ions (ionic radius=0.40 Å; CN=6). However, lattice expansion of TiNiN phases caused due to the substitution of Ti^{4+} ion (ionic radius 0.605 Å) by bigger Ni^{3+} ion (ionic radius 0.69 Å). Therefore, lattice parameter of TiMN phases increased linearly with the atomic number of the solute.

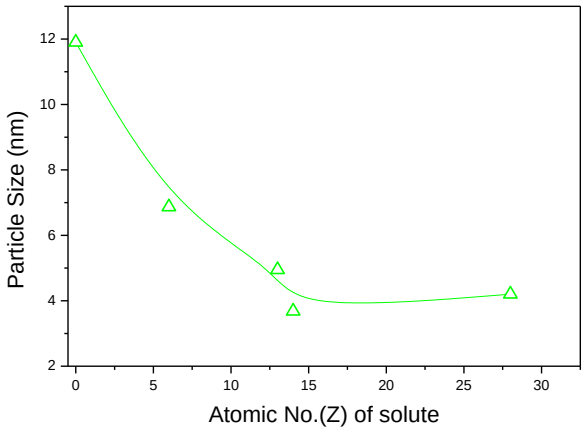

Fig.4. Variation of particle size of TiMN phases with atomic number of solute.

Fig.4 shows the variation of particle size of different Ti-base metal nitrides with the atomic number of the solutes. It is found that the particle size is isotropic and the particle size TiMN phases decrease rapidly up to Z=14 and attain a stable value up to Z= 28. This implies that the Z value of the intermediate solute plays a significant role in reducing the particle size and to attain a steady value.

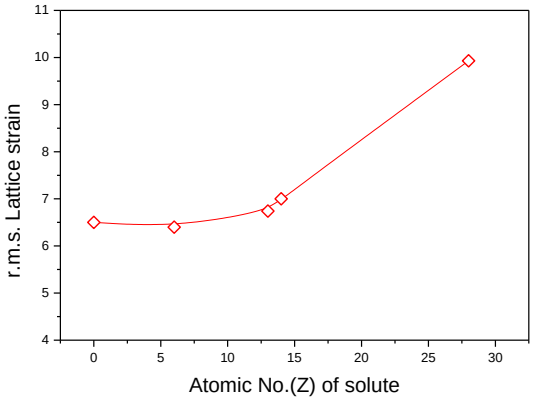

Fig.5. Variation of r.m.s. lattice strain of TiMN phases with atomic number of solute.

Variation of r.m.s. lattice strain of different TiMN phases is shown in Fig.5. Lattice strain values of all these phases are also found to be isotropic. The r.m.s. lattice strain almost remains constant up to Z=13 and then increases up to Z=28. This implies that Z value of solute has a great influence to attain stable lattice structure up to Z=13.

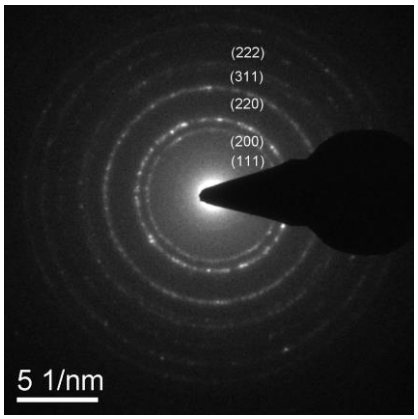

Fig.6. Selected area electron diffraction (SAED) pattern of nanocrystalline TiN powder after 9h of milling.

The selected area electron diffraction (SAED) (Fig. 6) pattern of 9h milled sample of TiN confirmed the formation of cubic TiN phase. Relative intensity ratios of the SEAD rings are at par with the XRD pattern. The proper appearance of SEAD rings reveals the formation cubic TiN phase without any contaminations either from elemental powders or from milling media.

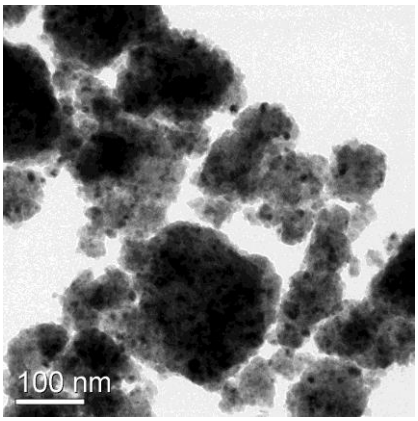

Fig. 7. HRTEM image of TiN particles after 9h of milling.

High-resolution transmission electron (HRTEM) micrograph of the 9h milled TiN sample (Fig. 7) reveals the presence of high-quality nanocrystals. These nanocrystals are isotropic in size and almost mono-dispersed particles having ~ 12nm average size. The crystallite size measured from HRTEM image is at par with that found from Rietveld's analysis.

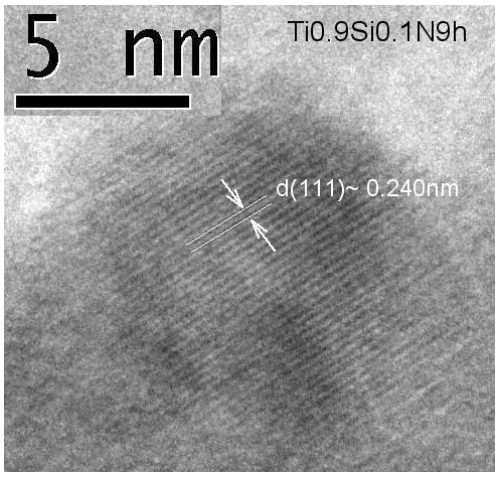

Fig. 8. HRTEM image of TiSiN particles after 9h of milling.

The interplanar spacing shown in Fig.8 is identified as (111) plane of cubic (Ti,Si)N phase with interplanar spacing d = 2.40 Å. These atomic planes are parallel and free from stacking faults.

5. CONCLUSIONS

i) Addition of small amount (0.1 mol fraction) of solute (C, Al, Si, Ni) to the elemental α-Ti accelerates the formation time of TiMN phases from 9h to 5h/7h.
ii) The lattice parameters of TiMN phases increased with atomic number of the solutes.
iii) Microstructure evolution of the 9h milled powder both by the Rietveld analysis and HRTEM reveals that TiN nanoparticles are almost mono-dispersed and their average crystallite size reduces to ~12nm.
iv) The TiSiN nanoparticles are free from stacking faults and almost free from lattice strain.

Acknowledgement

The authors wish to thank the University Grants Commission (UGC), India for granting UGC Minor research project. We are also grateful to SINP, Kolkata for providing the HRTEM facility.

REFERENCES:

[1] H. Zheng, K. Oka and J. D. Mackenzie, Mater. Res. Soc. Symp. Proc., 271(1992) pp 893.
[2]T. Graziani, A. Bellosi, J. Mater. Sci. Lett., 14 (1995) pp 1078.
[3] K. Kamiya, T. Nishijima, J. Am. Ceram. Soc., 79(9) (1990) pp 2750.
[4] H. C. Yi, J. J. Moore, J. Mater. Sci. 25 (1990) pp 1159.
[5] J. P. Dekker, P. J. Put, H. J. Veringa, J. Schoonman, J. Am. Ceram. Soc. 80 (3) (1997) pp 629.

[6] T. Yoshida, A. Kawasaki, K. Nakagawa, K. Akashi, J. Mater. Sci. 14 (1979) pp 1624.
[7] T. Sato, S. Yasuda, K. Usuki, T. Yoshioka, A. Okuwaki, J. Mater. Sci. 31(1990) pp 2495.
[8] C. H. Winter, P. J. McKarns, J. T. Scheper, Mater. Res. Soc. Symp. Proc. 95 (1998) pp 495.
[9] N. Liu, Y. D. Xu, H. Li, Z. H. Li, Y. Zhao, G. H. Li, L. D. Zhang, Mater. Sci. Technol.18 (2002) pp 586–590.
[10] G. I. Grigorov, K. G. Grigorov, M. Stayanova, J. L. Vignes, J. P. Langeron, P. Denjean, Appl. Phys. A 57 (1993) pp 195.
[11] J.T. Chen, J. Wang, F. Zhang, G.A. Zhang, X.Y. Fan, Z. G. Wu, P.X. Yan, J. Alloy Compd. 472 (2009) pp 91–96.
[12] Y.J. Lee, S.-W. Kang, Appl. Phys. Lett. 86 (2005) pp 071919.
[13] M. Zhou, Y. Makino, M. Nose, K. Nogi, Thin Solid Films 339 (1999) pp 203.
[14] A. Horling, L. Hultman, M. Oden, J. Sjolen, L. Karlsson, Surf. Coat.Technol. 191 (2005) pp 384.
[15] S. Kang, Pow. Metall 40 (1997) pp 139–142.
[16] L. Chen, W. Lengauer, K. Dreyer, Int. J. Refrac. Met. and Hard Mater. 18 (2000) pp 153–161
[17] R. M. German. "Liquid phase sintering". John Wiley and Sons, Inc., New York, 1985.
[18] B. Gómez, E. Gordo, E.M. Ruiz-Navas, J.M. Torralba, J. Achiev. Mater. and Manufac. Eng. 17 (1-2) (2006) pp 57-60.
[19] D.G. Liu, C.D. Gu, R. Chen, J.P. Tu, Surf. Coat. Technol. 205 (2010) pp 2386–2392.
[20] A. Bendavid, P.J. Martin, E.W. Preston, J. Cairney, Z.H. Xie, M. Hoffman, Surf. Coat. Technol. 201 (2006) pp 4139.
[21] Z. T. Yang, B. Yang, L.P. Guo, D.J. Fu, J. Alloy Compd. 473 (2009) pp 437.
[22] S. Veprek, S. Reiprich, Thin Solid Film. 268 (1995) pp 64.
[23] J. H. Park, S. H. Kwon, M. H. Lee, K.H. Kim, Electrochem. Solid-State Lett. 12 (2009) pp C13.
[24] H. R. Stock, M. Diesselberg, H. W. Zoch, Surf. Coat. Technol. 203 (2008) pp 717–720.
[25]L. Lutterotti, MAUD version2.26,(2010).http://www.ing.unitn.it/~luttero/maud.
[26] H. M. Rietveld, Acta Cryst. 22 (1967) pp 151-152.
[27] H. M. Rietveld, J. Appl. Cryst. 2 (1969) pp 65-71.
[28] H. Toraya, J. Appl. Cryst. 33 (2000) pp 1324-1328.
[29] B.E. Warren, X-ray Diffraction, Chap. 13, Addison-Wesley, Reading, (1969).
[30] D.B. Wiles, R.A. Young, J. Appl. Cryst. 14 (1981) pp 149-151.
[31] R.A. Young, D.B. Wiles, J. Appl. Cryst. 15 (1982) pp 430-438.
[32] R.A. Young, The Rietveld Method, edited by R.A. Young, pp. 1-38, Oxford University Press /IUCr, 1996.
[33] B. Ghosh, S.K. Pradhan, Mat. Chem. Phys. 120 (2010) pp 537–545.